Approaching a realistic force balance in geodynamo simulations

Rakesh K. Yadav[a,b,1], Thomas Gastine[b,c], Ulrich R. Christensen[b], Scott J. Wolk[a], and Katja Poppenhaeger[d,a]

[a]Harvard-Smithsonian Center for Astrophysics, Cambridge, MA 02138; [b]Max-Planck-Institut für Sonnensystemforschung, 37077 Göttingen, Germany; [c]Institut de Physique du Globe de Paris, Sorbonne Paris Cité, Université Paris-Diderot, UMR 7154 CNRS, F-75005 Paris, France; and [d]Astrophysics Research Center, Queen's University Belfast, BT7 1NN Belfast, United Kingdom

Edited by Peter L. Olson, Johns Hopkins University, Baltimore, MD, and approved September 13, 2016 (received for review June 6, 2016)

Earth sustains its magnetic field by a dynamo process driven by convection in the liquid outer core. Geodynamo simulations have been successful in reproducing many observed properties of the geomagnetic field. However, although theoretical considerations suggest that flow in the core is governed by a balance between Lorentz force, rotational force, and buoyancy (called MAC balance for Magnetic, Archimedean, Coriolis) with only minute roles for viscous and inertial forces, dynamo simulations must use viscosity values that are many orders of magnitude larger than in the core, due to computational constraints. In typical geodynamo models, viscous and inertial forces are not much smaller than the Coriolis force, and the Lorentz force plays a subdominant role; this has led to conclusions that these simulations are viscously controlled and do not represent the physics of the geodynamo. Here we show, by a direct analysis of the relevant forces, that a MAC balance can be achieved when the viscosity is reduced to values close to the current practical limit. Lorentz force, buoyancy, and the uncompensated (by pressure) part of the Coriolis force are of very similar strength, whereas viscous and inertial forces are smaller by a factor of at least 20 in the bulk of the fluid volume. Compared with nonmagnetic convection at otherwise identical parameters, the dynamo flow is of larger scale and is less invariant parallel to the rotation axis (less geostrophic), and convection transports twice as much heat, all of which is expected when the Lorentz force strongly influences the convection properties.

geodynamo | magnetohydrodynamics | planetary dynamos | turbulence | rotating convection

Sustained magnetism in astrophysical objects is due to the dynamo mechanism, which relies on the generation of electrical currents by fluid motion (1). The secular cooling of Earth's interior and the release of light elements at the boundary of the solid inner core provide buoyancy sources that drive convection, leading to the generation of electrical currents (2). It has been more than two decades since the idea of modeling the geomagnetic field using computer simulations was successfully demonstrated (3, 4). These pioneering simulations were able to reproduce the dipole-dominant nature of the geomagnetic field and showed reversals of the geomagnetic dipole. Since then, computer simulations have become a primary tool for studying the properties of the geomagnetic field (5–9).

The range of flow length scales present in the liquid outer core is enormous due to the very small viscosity of the fluid. To model this aspect in geodynamo simulations would require tremendous computing power that is not available even in the foreseeable future. Therefore, all geodynamo simulations must use unrealistically large viscosity to reduce the level of turbulence. One quantity that epitomizes this discrepancy is the Ekman number $E=\nu\Omega^{-1}D^{-2}$ (ν is the viscosity, Ω is Earth's rotation rate, and D is the thickness of the liquid outer core), which roughly quantifies the ratio of the viscous force F_V and the Coriolis force F_C. The Ekman number is about 10^{-15} in the core, whereas simulations typically use 10^{-4} (2).

The Coriolis force tends to suppress changes of the flow in the direction of the rotation axis, i.e., makes the flow nearly geostrophic (10, 11). This is known as the "Proudman–Taylor constraint" (PTC). Because the boundary of the fluid core is inclined relative to the direction of rotation (except at the poles), convective motions cannot be purely geostrophic, and therefore the PTC impedes convection (12). In the absence of a magnetic field, viscous force or inertial force F_I must compensate the part of the Coriolis force that cannot be balanced by the pressure force F_P. F_V or F_I may still be significantly smaller than the Coriolis force. For example, at the onset of nonmagnetic convection in a sphere, F_V is smaller than F_C by a factor $E^{1/3}$. Nonetheless, it is of the same order as $|\mathbf{F}_C+\mathbf{F}_P|$ and plays a key role in the force balance. The buoyancy force F_A (Archimedean) is comparable to F_V, and the state can be referred to as being in a VAC (Viscous, Archimedean, Coriolis) balance (13).

In Earth's core, the buoyancy force and the Lorentz force F_L due to the geomagnetic field are expected to be comparable to the Coriolic force (2, 14–16). This state is commonly referred to as a Magnetic, Archimedean, Coriolis (MAC) state. Here, the dynamo presumably selects a magnetic field that leads to an efficient relaxation of the PTC; this is expected to occur at $\Lambda\approx\mathcal{O}(1)$, where the Elsasser number is $\Lambda=B^2(\rho\mu\lambda\Omega)^{-1}$ (B is mean magnetic field, ρ is density, μ is magnetic permeability, and λ is magnetic diffusivity) (14, 15). Note that here we use the term MAC balance in the sense that F_L and F_A are of the same order as the uncompensated Coriolis force $|\mathbf{F}_C+\mathbf{F}_P|$, not necessarily the total Coriolis force.

Although a MAC state has long been expected from theoretical considerations, its existence in geodynamo simulations has not been demonstrated so far. A recent study of geodynamo

Significance

Flow in Earth's liquid core is expected to be primarily governed by the Coriolis force due to Earth's rotation, the buoyancy force driving the convection, and the Lorentz force due to the geomagnetic field. A relevant geodynamo model has to be in such a force balance. Contemporaneous simulations invoke high viscosities to suppress flow turbulence to keep the computational costs manageable. The unrealistically large viscosity in these simulations is a major concern. Here we show that the state-of-the-art simulations with a viscosity that is lower than in most simulations, but still much larger than in Earth's core, can approach a realistic force balance. Our simulations produce many properties that have been theoretically predicted in the past.

Author contributions: R.K.Y., T.G., and U.R.C. designed research; R.K.Y. performed research; R.K.Y. analyzed data; and R.K.Y., T.G., U.R.C., S.J.W., and K.P. wrote the paper.

The authors declare no conflict of interest.

This article is a PNAS Direct Submission.

[1]To whom correspondence should be addressed. Email: rakesh.yadav@cfa.harvard.edu.

This article contains supporting information online at www.pnas.org/lookup/suppl/doi:10.1073/pnas.1608998113/-/DCSupplemental.

models at an Ekman number of 10^{-4} explicitly calculated the value of the various forces (17). The authors show that the viscous force was actually comparable to the other forces. Furthermore, the analysis of convection properties suggested that a VAC state, rather than a MAC state, exists in contemporary geodynamo simulations (13). The presence of a VAC state promotes the idea that cost-efficient simulations might produce geodynamo-like features for the wrong reasons (2). A natural question then arises: How small should the viscosity be for a MAC state to appear? Due to the very nature of this question, a detailed parameter study is called for that systematically explores the parameter regime of geodynamo simulations.

Method

We carry out a detailed study of geodynamo models where we analyze data from our recent study (18) and carry out new simulations at more extreme values of the control parameters. The basic setup is geodynamo-like, and we consider a spherical shell where the ratio of the inner (r_i) and the outer (r_o) radius is 0.35. The thickness D of the shell is given by $r_o - r_i$. The convection in the shell is driven by a superadiabatic temperature contrast ΔT across the two boundaries. The shell rotates along the $\hat{z}$ axis with an angular frequency Ω. We work with nondimensional equations, and we use D as standard length scale, D^2/ν as time scale, ΔT as temperature scale, and $\sqrt{\rho\mu\lambda\Omega}$ as magnetic field scale.

We use the Boussinesq approximation, and the equations governing the velocity $\mathbf{u}$, magnetic field $\mathbf{B}$, and temperature perturbation T are

$$E\left(\frac{\partial \mathbf{u}}{\partial t}+\mathbf{u}\cdot\nabla\mathbf{u}\right)+2\hat{z}\times\mathbf{u}=-\nabla P+\frac{Ra\,E}{P_r}g(r)T\,\hat{\mathbf{r}}+\frac{1}{P_m}(\nabla\times\mathbf{B})\times\mathbf{B}+E\nabla^2\mathbf{u}, \quad [1]$$

$$\nabla\cdot\mathbf{u}=0, \quad [2]$$

$$\frac{\partial T}{\partial t}+\mathbf{u}\cdot\nabla T=\frac{1}{P_r}\nabla^2 T, \quad [3]$$

$$\frac{\partial \mathbf{B}}{\partial t}=\nabla\times(\mathbf{u}\times\mathbf{B})+\frac{1}{P_m}\nabla^2\mathbf{B}, \quad [4]$$

$$\nabla\cdot\mathbf{B}=0, \quad [5]$$

where $g(r)$ is the gravity that varies as r/r_o, and P is the pressure. The control parameters that govern the system are

$$\text{Prandtl number } P_r=\frac{\nu}{\kappa}, \quad [6]$$

$$\text{magnetic Prandtl number } P_m=\frac{\nu}{\lambda}, \quad [7]$$

$$\text{Rayleigh number } Ra=\frac{\alpha\, g_o\, D^3\Delta T}{\nu\,\kappa}, \quad [8]$$

where α is the thermal expansivity, g_o is the gravity at the outer boundary, and κ is the thermal diffusivity.

Both boundaries have fixed temperature, are no-slip, and are electrically insulating. The open-source code MagIC (available at https://www.github.com/magic-sph/magic) is used to simulate the models (19). The code uses spherical harmonic decomposition in latitude and longitude and Chebyshev polynomials in the radial direction. MagIC uses the SHTns library (20) to efficiently calculate the spherical harmonic transforms. Because we use nondimensional equations, the relative influence of viscosity is mainly expressed by the value of the Ekman number. To explore the effect of the magnetic field, we perform hydrodynamic (HD) simulations, i.e., without a magnetic field, in parallel to the dynamo models.

The results of simulations with $E=10^{-4}, 10^{-5}$ are taken from our earlier study (18) and are extended here to runs at $E=10^{-6}$. In all of our simulations, the fluid Prandtl number P_r is unity. The magnetic Prandtl number P_m is also unity for cases with $E=10^{-4}$ and $E=10^{-5}$. At $E=10^{-6}$, we ran five dynamo simulations with P_m of 2, 1, 0.5, 0.5, and 0.4 (in order of increasing Ra). To reduce the time spent in calculating the transient stages for $E=10^{-6}$ simulation with highest Ra, we use a scaled $E=10^{-5}$ dynamo simulation as initial condition. The scaling factors for magnetic field and velocity are calculated using the scaling laws by Christensen and Aubert (21). Furthermore, the other $E=10^{-6}$ simulations at lower Ra use an initial condition from a higher Ra case. Data tables that contain useful globally averaged quantities, grid resolutions, and simulation run-time are provided as Datasets S1 and S2.

Results

We begin our analysis by explicitly calculating the various forces involved in the system, namely, Coriolis force F_C, buoyancy (Archimedian) forces F_A, Lorentz force F_L, inertial force F_I, viscous force F_V, and pressure gradient force F_P. We compare the root-mean-square values of these forces, averaged in space and in time. Because our main goal is to compare the importance of various forces for the flow dynamics, care must be exercised in choosing the appropriate quantities. The spherically symmetric component of any force is dynamically irrelevant; we thus exclude the harmonic order $m = 0$ component from the force values. The PTC implies that the Coriolis force is largely compensated by the pressure gradient. For our purpose, we only concentrate on that part of F_C that is not balanced by the pressure gradient force. Therefore, we consider $\mathbf{F}_C+\mathbf{F}_P$ rather than $\mathbf{F}_C$ alone.

Because we use no-slip boundary conditions, Ekman layers are formed at the boundaries (12). Within these layers, the viscous force is dominant. Due to the larger viscosity, contemporary geodynamo simulations have much thicker Ekman boundary layers than those present in Earth's core. This leads to a rather substantial contribution of the boundary layer viscous force to the total viscous force (e.g., see refs. 22 and 23). Therefore, we choose to exclude thin boundary layers, one below the outer boundary and one above the inner boundary, from the force calculation. The thickness of the excluded layers is 1%, 2%, and 3% of the shell thickness for $E=10^{-6}$, 10^{-5}, and 10^{-4}, respectively. The chosen thickness of the layers is a rough estimate, and the values are such that any larger value does not lead to further appreciable change in the bulk viscous force. For the sake of consistency, boundary layers are excluded from averaging procedure for all other force types as well. Sometimes it is argued that Ekman suction in the viscous boundary layer (12) plays an essential role for creating flow helicity as an important prerequisite for magnetic field generation (24). However, we note that geodynamo simulation with a stress-free boundary that lacks Ekman suction shows quite similar results compared with models with rigid boundaries (9, 25); hence viscous boundary layer effects do not seem to play an essential role.

The various forces calculated from the simulations are portrayed in Fig. 1 A–C as a function of the convective supercriticality Ra/Ra_c (Ra_c is the critical Ra where convection starts). First, notice that our choice of using $\mathbf{F}_C+\mathbf{F}_P$ rather than $\mathbf{F}_C$ makes a substantial difference, because both F_C and F_P are very strong, but they cancel each other to a large extent. Therefore, to the zeroth-order, the system is in a geostrophic state, where F_C and F_P are dominant. The first-order deviations are balanced by other weaker forces; these may be Lorentz, viscous, or inertial forces. One may call this state a "quasi-geostrophic" one (26). In the $E=10^{-4}$ simulations, the various forces remain comparable to each other to within an order of magnitude. This series of runs spans a large range of Ra/Ra_c, covering the transition from dipole-dominant dynamos to multipolar ones (occurring at around $Ra/Ra_c \approx 30$ for $E=10^{-4}$). With decreasing Ekman number, the transition shifts to higher values of Ra/Ra_c (27), which are not reached in our simulations with $E \le 10^{-5}$. The latter all have a dominantly dipolar magnetic field. As convection becomes more turbulent, the inertial force eventually becomes the most dominant force in our $E=10^{-4}$ simulations. For low convective supercriticalities ($Ra/Ra_c < 10$), F_C and F_A are comparable for all E. The Lorentz force F_L starts to match these two forces as Ra increases. At $E=10^{-5}$ and, more obviously, at $E=10^{-6}$, a clear hierarchy of forces becomes apparent for $Ra/Ra_c \gtrsim 10$. Inertial and viscous forces are at least a factor of 10 weaker than the others. Lorentz, Archimedean, and (uncompensated) Coriolis forces are very similar in amplitude and

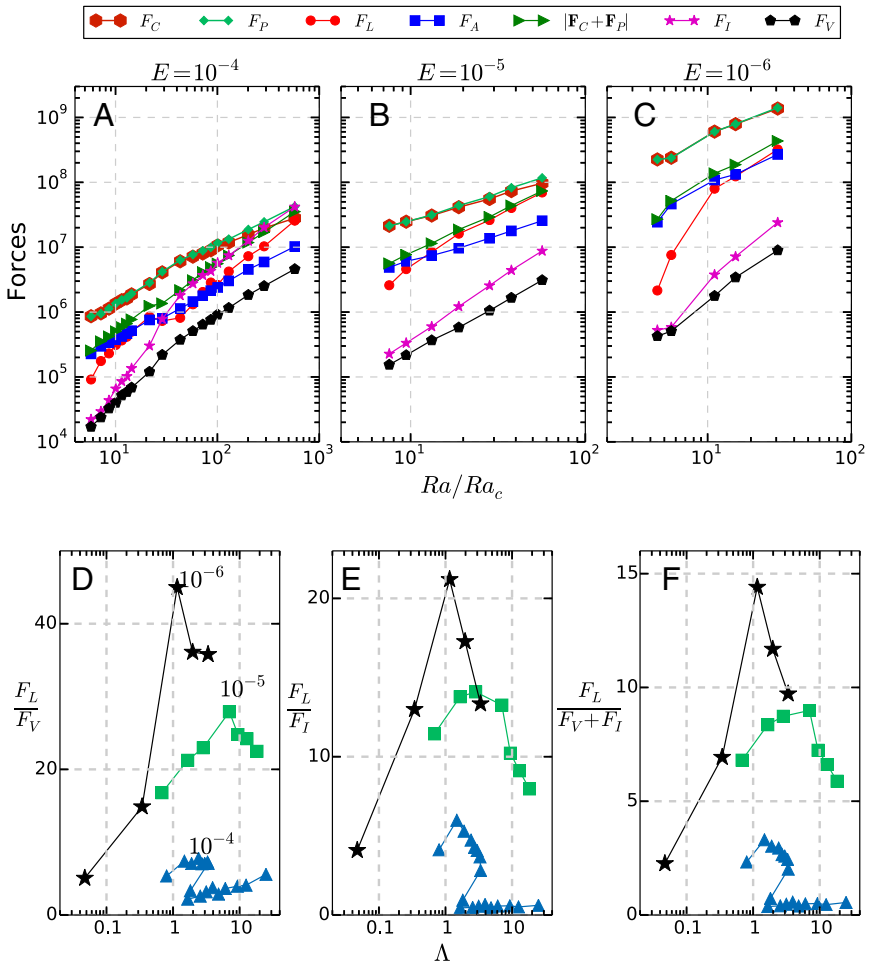

Fig. 1. (*A*–*C*) Variation of the forces governing the dynamo simulations as a function of the convective supercriticality Ra/Ra_c. The Ra_c values assumed for (*A*) $E = 10^{-4}$, (*B*) $E = 10^{-5}$, and (*C*) $E = 10^{-6}$ are 6.96×10^5, 1.06×10^7, and 1.79×10^8, respectively (21). The magnitudes of Coriolis force and the pressure gradient force are similar for most Rayleigh numbers, and the data points overlap. The legend describing the data in *A*–*C* is shown at the top. (*D*–*F*) Behavior of various force ratios as a function of the dynamo generated Elsasser number Λ: (*D*) F_L/F_V, (*E*) F_L/F_I, and (*F*) $F_L/(F_V + F_I)$. The different colors in *D*–*F* represent different Ekman numbers that are indicated in *D*. The curves connecting the $E = 10^{-4}$ data points in *D*–*F* follow increasing *Ra* trend. Therefore, as the dipolar dynamos with $E = 10^{-4}$ become unstable at certain Λ, the curve turns back even though the *Ra* increases.

balance each other; that is, the bulk of the fluid is in a dynamical MAC state. We reiterate that, because Coriolis and pressure forces are individually rather strong, the zeroth-order force balance is largely geostrophic, and the notion of a MAC state in our simulations is a first-order effect.

We plot the ratio of F_L and F_V as a function of the Elsasser number Λ in Fig. 1*D*. In simulations with $E = 10^{-4}$, as the dynamo-generated field strength increases, the ratio F_L/F_V reaches a maximum of about 8. Lowering E to 10^{-5} and 10^{-6} increases this maximum ratio to about 30 and 45, respectively. The largest ratios between F_L and F_V are reached for cases with Elsasser numbers of order 1. As shown in Fig. 1*E*, the ratio F_L/F_I also follows the same qualitative trend as F_L/F_V. Note that a MAC state can be disturbed by the viscous force; however, with increasing flow turbulence, the inertial force can also do the same (28). Therefore, it is appropriate to compare Lorentz force and the sum of viscous and inertial forces. As Fig. 1*F* shows, such a comparison provides a succinct way of highlighting the overall dominance of the Lorentz force. In this context, it is worth pointing out that assuming a higher magnetic Prandtl number may help to increase the strength of the magnetic field and, in turn, its influence on the flow (21, 25, 29). However, whether such an approach is justified or not remains to be tested.

The trends in the forces highlighted above have important consequences for the properties of convection. When a VAC balance holds in rapidly rotating convection, the characteristic flow length scale l_u is proportional to $D\,E^{1/3}$; that is, length scales become smaller with decreasing E (2, 13, 30). As shown in Fig. 2 *A*–*D*, the convective structures in our HD simulations do follow this trend qualitatively as E decreases. On the other hand, in the MAC regime, l_u is expected to be similar to the system size and to remain independent of E (2, 16, 31). For simulation with $E \geq 10^{-4}$, both HD and dynamo cases have rather similar convective length scales (Fig. 2 *E* and *F*). At $E = 10^{-5}$, the dynamo case has a higher tendency for elongated structures in the radial direction and fewer upwellings and downwellings in azimuthal direction (Fig. 2*G*) compared with the HD case (Fig. 2*C*). At $E = 10^{-6}$, the dynamo case has significantly larger length scales (Fig. 2*H*) than the corresponding HD setup (Fig. 2*D*). This increased influence of the magnetic field is also reflected in the total magnetic energy, which exceeds the total kinetic energy more and more as E is decreased (Fig. S1). Another interesting feature in the $E = 10^{-6}$ dynamo case is the presence of a layer of small-scale convection near the outer boundary; this is caused by a relatively weaker Lorentz force in these regions (Fig. S2). We conclude that hints of a MAC regime appear at $E = 10^{-5}$ (32, 33), but this regime

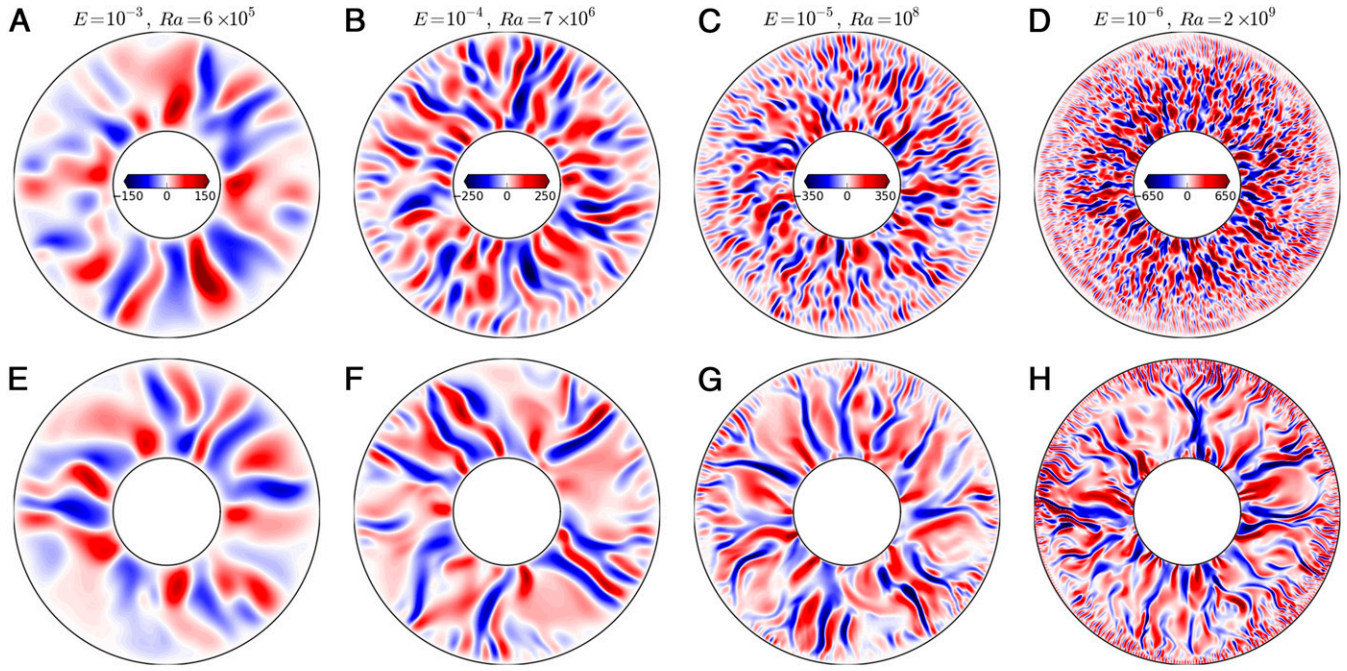

Fig. 2. (*A*–*D*) Radial velocity, given in terms of the Reynolds number ($u\,D/\nu$, where u is the local velocity), in the equatorial plane of the HD simulations. (*E*–*H*) The same for the corresponding magnetohydrodynamic cases. (*A* and *E*) $E = 10^{-3}$, $Ra = 6 \times 10^5$; (*B* and *F*) $E = 10^{-4}$, $Ra = 7 \times 10^6$; (*C* and *G*) $E = 10^{-5}$, $Ra = 10^8$; and (*D* and *H*) $E = 10^{-6}$, $Ra = 2 \times 10^9$. The Rayleigh number of all of the cases shown is about 10 times Ra_c. The color maps are saturated at values lower than the extrema to highlight fainter structures.

is more prominent at $E = 10^{-6}$. Furthermore, in a single system, there might be regions where a MAC state prevails whereas, in some other regions, it may not (also see refs. 29 and 34).

In Fig. 3, we present the three-dimensional morphology of the convection in the HD and in the dynamo case for the lowest-viscosity simulation with the largest ratio of Lorentz force to viscous and inertial forces. The HD setup has small axially aligned tube-like convection columns. In the dynamo case, however, the convection occurs in the form of thin sheets stretched in the cylindrically radial direction. It is also clear that, compared with the HD case, the convective structures vary more along the rotation axis. Both features demonstrate the influence of the Lorentz forces on the convention morphology.

Another way to quantify the relaxed Proudman–Taylor constraint in the dynamo cases is to analyze the total heat transferred from the bottom boundary to the top; this stems from the notion that rotation quenches the efficiency of convection by suppressing motions along the rotation axis (12). Any relaxation of this constraint will lead to a gain in heat transfer efficiency. We use the ratio of the Nusselt number Nu (ratio of the total heat and the conductive heat transferred from the bottom to the top boundary) for dynamo and HD cases as a function of the dynamo-generated average magnetic field strength (Fig. 4). At $E = 10^{-4}$, the Nu ratio remains close to unity, implying that the convective heat transport in dynamo and HD cases is similar. At $E = 10^{-5}$, the Nu ratio peaks for $\Lambda \approx 3$ and reaches a value of about 1.3 (18). This enhancement of heat transport by the presence of a magnetic field is more pronounced when we further decrease E to 10^{-6}. Here, the heat flow is doubled for $\Lambda \approx 1$. Comparing this figure with Fig. 1 *D*–*F* highlights that the gain in the heat transfer efficiency in the dynamo cases is largest when the Lorentz force is maximally dominant over viscous and inertial forces.

Discussion

To summarize, we used a systematic parameter study to test the existence of a dynamical state in dynamo simulations where

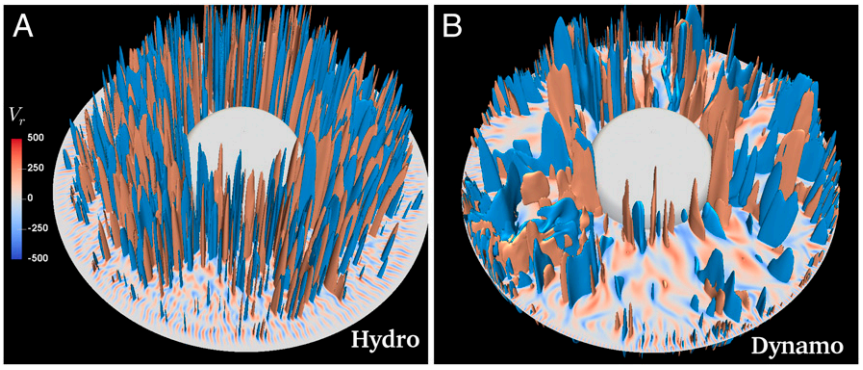

Fig. 3. Perspective view of (*A*) an HD case and (*B*) a dynamo case with $E = 10^{-6}$, $P_m = 0.5$, and $Ra = 2 \times 10^9$. The radial velocity on the equatorial plane is given in terms of the Reynolds number. The blue and light orange contours represent radial velocity of −300 and 300, respectively.

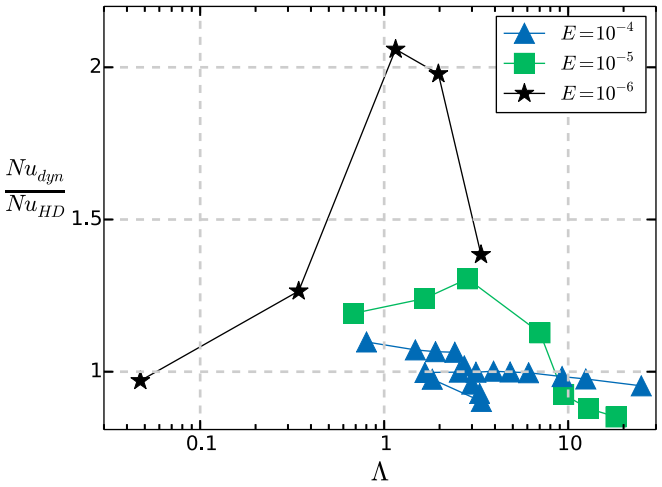

Fig. 4. Ratio of Nusselt number *Nu* of dynamo and HD cases (with otherwise same control parameters) as a function of the Elsasser number.

magnetic forces play a crucial role together with Coriolis and buoyancy forces (MAC state), as is expected to be present in Earth's core. We lowered the viscosity to a small value, close to the limit allowed by today's computational resources, and found that Lorentz forces become equal in strength to (uncompensated) Coriolis and buoyancy forces and, for a limited range of Rayleigh numbers, far exceed viscous and inertial forces. The increased influence of the Lorentz force leads to large-scale convection, substantial axial variation in the convection structures, and a 100% increase in the heat transfer efficiency compared with the corresponding HD setup. All of these features are expected theoretically (2). For higher viscosity values, the convection is much less affected by the magnetic field (17).

We note that, in our simulations the Lorentz force is substantially smaller than the Coriolis force or the pressure force (taken individually). Hence, the state can be called quasi-geostrophic (26). Nonetheless, a completely geostrophic state is impossible, and the essential question is what balances the residual Coriolis force. Because these are the Lorentz and Archimedean forces, with an insignificant role for viscosity and inertia, it is also justified to speak of a MAC balance. We also note that, although a MAC balance is satisfied globally, this does not imply that the residual Coriolis force, Lorentz force, and buoyancy force are pointwise of the same magnitude. For example, strong Lorentz forces seem to be rather localized (Fig. S2), as found in previous studies (e.g., ref. 34). In regions where the Lorentz force is weak, the balance could be almost perfectly geostrophic, or buoyancy alone could balance the residual Coriolis force.

Our results show some similarities with earlier studies done in a similar context. Larger-scale convection in dynamo simulations compared with their HD counterparts has been reported in rotating convection in Cartesian geometry (35); there, the dynamo simulation with $E=10^{-6}$ showed about 60% increase in *Nu*. A recent laboratory experiment of rotating magnetoconvection (imposed magnetic field) in a cylinder also showed about 30% increase in *Nu* due to the presence of the magnetic field (at $E=4\times10^{-6}$ and $\Lambda\approx2$) (36).

In the context of geodynamo simulations, studies at Ekman numbers comparable to the lowest value used in our study have been reported before. A substantial change in the convection length scale due to the dynamo-generated magnetic field was found, but it only occurred in cases with constant heat flux boundary conditions (37). In contrast, we find the same enlargement of flow length scales also for fixed temperature conditions. Differences in the model setup and parameter values prevent us from elucidating the exact cause for these differences. Miyagoshi et al. (38, 39) also performed geodynamo simulations with $E\approx10^{-6}$ (in our definition) and observed a "dual-convection" morphology where the deeper convecting regions had thin cylindrically radial structures and the outer regions had very large-scale spiraling features embedded into a prominent zonal flow. We also found such convection morphology at $E=10^{-6}$, in both HD and dynamo simulations, but only at low Rayleigh numbers ($Ra/Ra_c<10$). Again, our simulations and these studies (38, 39) are significantly different in model details; for example, they assumed that gravity dropped sharply with radius, whereas, in our case, it linearly increases from the inner to the outer boundary, as is appropriate for Earth's core. A geodynamo simulation at the lowest Ekman number reached so far has been performed by Nataf and Schaeffer (40) and shows rather small flow scales. Because hardly any details of the simulation are available, it is difficult to assess the reasons. Possibly, strong driving could make inertial forces significant, leading to a compromised MAC state.

Our parameter study has shown that, at an Ekman number of 10^{-6}, a MAC state, as is expected in Earth's core, is very nearly reached, albeit only in a limited range of moderate Rayleigh numbers. As a consequence, the magnetic dipole dominates more strongly over higher multipoles at the outer boundary than it does in the geomagnetic field. Furthermore, the dipolar mode in the $E=10^{-6}$ simulation appears to be rather stable and does not show indications of reversals, unlike the geomagnetic field. In previous dynamo simulations, the onset of reversals has been associated with a growing influence of the inertial force at higher Rayleigh number (21, 34). We expect that pushing the Ekman number to even lower values would expand the range where a MAC state exists toward more strongly supercritical values of the Rayleigh number (41), but this does not necessarily imply that inertia becomes significant. It remains an open question whether inertial effects are responsible for triggering reversals in the geodynamo (which would then not be in a pure MAC state), or if some other effects associated with a more strongly supercritical Rayleigh number play a role in reversals. Another challenge to tackle is the extreme value of the magnetic Prandtl number, which is also fundamentally important for the geodynamo mechanism (2). In Earth, P_m is expected to be about 10^{-6}, implying a large difference in the typical length scales of the velocity and the magnetic field (the latter varying on larger scales). To have a magnetic Reynolds number large enough to sustain a dynamo at low P_m, the convection must generate a Reynolds number in excess of a million. To keep the system rotationally dominant and very turbulent, one must inevitably decrease the Ekman number to much smaller values than what we could reach in this study. Therefore, a way forward in future is to strive for even lower Ekman numbers and lower magnetic Prandtl numbers to approach the conditions of the geodynamo.

ACKNOWLEDGMENTS. We thank the two anonymous referees for very constructive comments. Funding from NASA (through the Chandra Grant GO4-15011X) and Deutsche Forschungsgemeinschaft (through SFB 963/A17) is acknowledged. S.J.W. was supported by NASA Contract NAS8-03060. Simulations were performed at Gesellschaft für wissenschaftliche Datenverarbeitung mbH Göttingen (GWDG) and Rechenzentrum Garching der Max-Planck-Gesellschaft (RZG).

1. Brandenburg A, Subramanian K (2005) Astrophysical magnetic fields and nonlinear dynamo theory. *Phys Rep* 417(1-4):1–209.
2. Roberts PH, King EM (2013) On the genesis of the Earth's magnetism. *Rep Prog Phys* 76(9):096801.
3. Glatzmaier GA, Roberts PH (1995) A three-dimensional convective dynamo solution with rotating and finitely conducting inner core and mantle. *Phys Earth Planet Inter* 91(1):63–75.
4. Glatzmaier GA, Roberts PH (1995) A three-dimensional self-consistent computer simulation of a geomagnetic field reversal. *Nature* 377(6546):203–209.
5. Christensen UR, Tilgner A (2004) Power requirement of the geodynamo from ohmic losses in numerical and laboratory dynamos. *Nature* 429(6988):169–171.
6. Gubbins D, Sreenivasan B, Mound J, Rost S (2011) Melting of the Earth's inner core. *Nature* 473(7347):361–363.

7. Aubert J, Finlay CC, Fournier A (2013) Bottom-up control of geomagnetic secular variation by the Earth's inner core. *Nature* 502(7470):219–223.
8. Olson P, Hinnov LA, Driscoll PE (2014) Nonrandom geomagnetic reversal times and geodynamo evolution. *Earth Planet Sci Lett* 388:9–17.
9. Aubert J (2014) Earth's core internal dynamics 1840–2010 imaged by inverse geodynamo modelling. *Geophys J Int* 197(3):1321–1334.
10. Proudman J (1916) On the motion of solids in a liquid possessing vorticity. *Proc R Soc Lond A Math Phys Eng Sci* 92(642):408–424.
11. Taylor GI (1923) Experiments on the motion of solid bodies in rotating fluids. *Proc R Soc Lond A Math Phys Eng Sci* 104(725):213–218.
12. Greenspan HP (1968) *The Theory of Rotating Fluids* (Cambridge Univ Press, New York).
13. King EM, Buffett BA (2013) Flow speeds and length scales in geodynamo models: The role of viscosity. *Earth Planet Sci Lett* 371:156–162.
14. Chandrasekhar S (1954) The instability of a layer of fluid heated below and subject to the simultaneous action of a magnetic field and rotation. *Proc R Soc Lond A Math Phys Sci* 225(1161):173–184.
15. Stevenson DJ (1979) Turbulent thermal convection in the presence of rotation and a magnetic field: A heuristic theory. *Geophys Astrophys Fluid Dyn* 12(1):139–169.
16. Starchenko S, Jones C (2002) Typical velocities and magnetic field strengths in planetary interiors. *Icarus* 157(2):426–435.
17. Soderlund KM, King EM, Aurnou JM (2012) The influence of magnetic fields in planetary dynamo models. *Earth Planet Sci Lett* 333:9–20.
18. Yadav RK, Gastine T, Christensen UR, Duarte L, Reiners A (2016) Effect of shear and magnetic field on the heat-transfer efficiency of convection in rotating spherical shells. *Geophys J Int* 204(2):1120–1133.
19. Wicht J (2002) Inner-core conductivity in numerical dynamo simulations. *Phys Earth Planet Inter* 132(4):281–302.
20. Schaeffer N (2013) Efficient spherical harmonic transforms aimed at pseudospectral numerical simulations. *Geochem Geophys Geosyst* 14(3):751–758.
21. Christensen UR, Aubert J (2006) Scaling properties of convection-driven dynamos in rotating spherical shells and application to planetary magnetic fields. *Geophys J Int* 166(1):97–114.
22. Stellmach S, et al. (2014) Approaching the asymptotic regime of rapidly rotating convection: boundary layers versus interior dynamics. *Phys Rev Lett* 113(25):254501.
23. Plumley M, Julien K, Marti P, Stellmach S (2016) The effects of Ekman pumping on quasi-geostrophic Rayleigh–Bénard convection. *J Fluid Mech* 803:51–71.
24. Davidson P, Ranjan A (2015) Planetary dynamos driven by helical waves–II. *Geophys J Int* 202(3):1646–1662.
25. Yadav RK, Gastine T, Christensen UR (2013) Scaling laws in spherical shell dynamos with free-slip boundaries. *Icarus* 225(1):185–193.
26. Calkins MA, Julien K, Tobias SM, Aurnou JM (2015) A multiscale dynamo model driven by quasi-geostrophic convection. *J Fluid Mech* 780:143–166.
27. Kutzner C, Christensen U (2002) From stable dipolar towards reversing numerical dynamos. *Phys Earth Planet Inter* 131(1):29–45.
28. Hughes DW, Cattaneo F (2016) Strong-field dynamo action in rapidly rotating convection with no inertia. *Phys Rev E Stat Nonlin Soft Matter Phys* 93(6):061101.
29. Dormy E (2016) Strong-field spherical dynamos. *J Fluid Mech* 789:500–513.
30. Jones CA, Soward AM, Mussa AI (2000) The onset of thermal convection in a rapidly rotating sphere. *J Fluid Mech* 405:157–179.
31. Jones CA, Roberts PH (2000) Convection-driven dynamos in a rotating plane layer. *J Fluid Mech* 404:311–343.
32. Takahashi F, Shimizu H (2012) A detailed analysis of a dynamo mechanism in a rapidly rotating spherical shell. *J Fluid Mech* 701:228–250.
33. Teed RJ, Jones CA, Tobias SM (2015) The transition to Earth-like torsional oscillations in magnetoconvection simulations. *Earth Planet Sci Lett* 419:22–31.
34. Sreenivasan B, Jones CA (2006) The role of inertia in the evolution of spherical dynamos. *Geophys J Int* 164(2):467–476.
35. Stellmach S, Hansen U (2004) Cartesian convection driven dynamos at low Ekman number. *Phys Rev E Stat Nonlin Soft Matter Phys* 70(5 Pt 2):056312.
36. King EM, Aurnou JM (2015) Magnetostrophic balance as the optimal state for turbulent magnetoconvection. *Proc Natl Acad Sci USA* 112(4):990–994.
37. Sakuraba A, Roberts PH (2009) Generation of a strong magnetic field using uniform heat flux at the surface of the core. *Nat Geosci* 2(11):802–805.
38. Miyagoshi T, Kageyama A, Sato T (2010) Zonal flow formation in the Earth's core. *Nature* 463(7282):793–796.
39. Miyagoshi T, Kageyama A, Sato T (2011) Formation of sheet plumes, current coils, and helical magnetic fields in a spherical magnetohydrodynamic dynamo. *Phys Plasmas* 18(7):072901.
40. Nataf HC, Schaeffer N (2015) Turbulence in the core. Treatise on Geophysics (Elsevier, New York), Vol 8, 2nd ed, pp 161–181.
41. Christensen UR, Aubert J, Hulot G (2010) Conditions for Earth-like geodynamo models. *Earth Planet Sci Lett* 296(3):487–496.